KINETICS, CATALYSIS, AND REACTION ENGINEERING

# Hydrogen Production and Carbon Formation during the Steam Reformer of Heptane in a Novel Circulating Fluidized Bed Membrane Reformer

**Zhongxiang Chen,* Yibin Yan, and Said S. E. H. Elnashaie**

*Department of Chemical Engineering, Auburn University, Auburn, Alabama 36849-5127*

Hydrogen production and carbon formation during the steam reforming of heptane over nickel-based catalyst are investigated in a circulating fluidized bed membrane reformer (CFBMR) at 723−823 K and 101.3−2026 kPa. A random carbon deposition and catalyst deactivation model is developed to account for the effect of carbon deposition on the overall reforming kinetics. The results show that the deposited carbon can be efficiently gasified by steam, hydrogen, carbon dioxide, or oxygen in this novel CFBMR, making carbon-free operation practically possible, especially when steam to carbon feed ratio is higher than 2.5 mol/mol. The use of hydrogen permselective membranes breaks the equilibrium barriers associated with the reversible reforming reactions and increases the hydrogen yield significantly. The introduction of oxygen into the adiabatic reformer can efficiently supply the heat necessary for the endothermic steam reforming through the exothermic oxidation, making an autothermal condition possible for the efficient production of hydrogen.

## Introduction

Hydrogen is forecast to become one of two principal energy carriers (with electricity) in the 21st century.[1,2] Currently, there are a number of catalytic and noncatalytic approaches for the production of hydrogen in industries.[3] Steam reforming of hydrocarbons, especially natural gas, is the largest and the most economical way to produce hydrogen.[1,3,4] In some countries where natural gas is not abundant such as Japan and the United States, steam reforming of higher hydrocarbons is the most important process for hydrogen production. [4,5,6] Steam reforming of hydrocarbons suffers from the carbon formation (coking), which deactivates the catalyst.[1,4,5,7−14] A number of investigations have shown that the rate of carbon formation is largely dependent on the chemical composition of the catalyst as well as its preparation procedure. [15,16] For steam reforming of hydrocarbons over commercial nickel catalysts, three main kinds of carbon or coke species were observed: pyrolytic carbon, which is usually formed through the cracking of hydrocarbons at temperatures above 600 °C and deposition of carbon precursors; encapsulated carbon, which is formed by slow polymerization of unsaturated hydrocarbon on nickel surface at temperatures lower than 500 °C; and filamentous or whiskerlike carbon, which is produced by diffusion of carbon into nickel crystals, detachment of nickel from the support, and growth of whiskers with nickel on the top of the catalyst.[10,11,13,17] Pyrolytic and encapsulated carbons encapsulate the catalyst particles and therefore deactivate the catalyst. Although the whiskerlike carbon does not deactivate the catalysts directly, it can grow on the nickel surface, causing the breakdown of the catalyst and blockage of the reformer tubes and leads to an increase in pressure drop.[7,11,13] The net carbon deposition is the difference between the carbon formation and carbon gasification. The carbon deposition may be controlled using optimal catalysts with dopants such as potassium, magnesia, urania, or molybdenum[9,11,12] or using high steam-to-carbon feed ratios.[4,6,13,18]

In this paper, a catalyst deactivation model is developed for commercial nickel reforming catalyst. This model is incorporated into an overall reformer model in order to study the carbon formation and hydrogen production by steam reforming of heptane in a circulating fluidized bed membrane reformer (CFBMR). [19−22] As shown in Figure 1, there are a number of palladium-based hydrogen permselective membrane tubes and dense perovskite oxygen permselective membrane tubes in the reformer. Between these membrane tubes, the nickel reforming catalyst is fast fluidized and steam reforming of heptane takes place. The product hydrogen permeates selectively through the hydrogen membranes and is carried away by sweep gas such as steam. Air is fed into the oxygen selective membrane tubes where oxygen permeates into the reaction side for oxidative reforming of hydrocarbons. The deactivated catalyst is carried out of the reformer, regenerated by burning the carbon along the exit line using excess air, and then separated in a gas−solid separator. The regenerated catalyst is recycled to the riser reformer. Previous investigations have shown this process would seem to be more efficient and flexible for a wide range of hydrocarbons.[19−22]

* To whom correspondence should be addressed. E-mail: chenzho@auburn.edu. Tel.: 1-334-844-2051. Fax: 1-334-844-2063.

10.1021/ie034198i CCC: $27.50 
Published on Web 02/14/2004

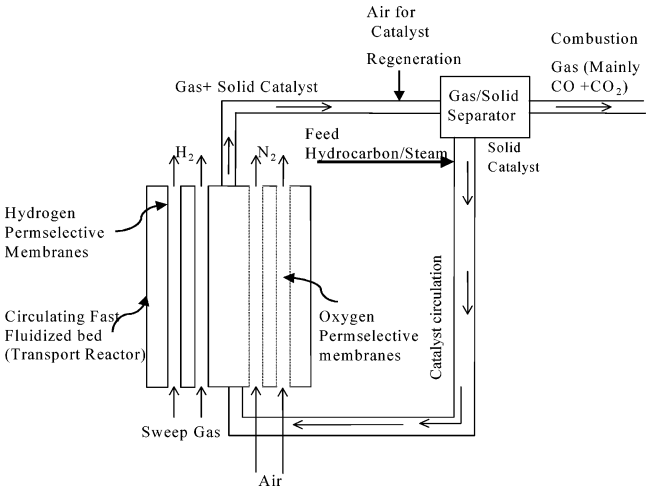


**Figure 1.** Novel process with a circulating fluidized bed membrane reformer (CFBMR).

### Catalyst Deactivation Model

A random carbon deposition model is developed according to the following steps: (a) Hydrocarbon is adsorbed on the catalyst surface to produce gas-phase products or to form precursors of coke/protocoke (dehydrogenated intermediates), which is mobile. (b) The protocoke deposits randomly on the nickel catalyst, on either the coked or uncoked sites. (c) The coking process can be schematically represented by the following.

$$C_nH_m \xrightarrow{r} CH_x \text{ (protocoke)} \xrightarrow{r_d} \text{carbon (or coke)} \quad \text{(for heptane, } n = 7 \text{ and } m = 16) \quad (1)$$

denoting $C^*$ and $C_k$ as the concentrations of protocoke and deposited coke, respectively; $r$ and $r_d$ as the protocoke formation rate and coke deposition rate, respectively; $S$ and $S_0$ as the concentrations of active sites per gram of catalyst at reaction time $t$ and initially, respectively. Starting with the material balance for protocoke and coke on the catalyst, we can write the following equations for $C^*$ and $C_k$:

$$\frac{dC^*}{dt} = r(S,P_{C_nH_m},...) - r_d(S_0,C^*) \quad (2)$$

$$\frac{dC_k}{dt} = r_d(S_0,C^*) \quad (3)$$

Assuming that the growth of protocoke into coke on the catalyst is fast, the pseudo-steady-state approximation can be used for the protocoke:

$$\frac{dC^*}{dt} = r(S,P_{C_nH_m},...) - r_d(S_0,C^*) = 0 \quad (4)$$

Since protocoke is formed from the adsorbed hydrocarbon, the formation rate can be assumed to be proportional to the concentration of adsorption sites. Therefore, the formation rate of protocoke is given by

$$r(S,P_{C_nH_m},...) = \frac{S}{S_0} r_0(S_0,P_{C_nH_m},...) \quad (5)$$

where $r_0$ is the initial formation rate of protocoke. Equation 3 can therefore be written as

$$\frac{dC_k}{dt} = \frac{S}{S_0} r_0(S_0,P_{C_nH_m},...) \quad (6)$$

If the active site coverage by carbon is the main cause of catalyst deactivation during the steam reforming of hydrocarbons, the catalyst activity $\phi$ may be written as

$$\phi = S/S_0 \quad (7)$$

Since the loss of the active sites is equal to the change of the active sites on the catalyst, we get

$$[-r_d(S_0,C^*)]W_{cat}\Delta t\alpha\frac{S}{S_0} = W_{cat}\Delta S \quad (8)$$

where $W_{cat}$ is the catalyst weight, $\Delta t$ is the segment of reaction time, and $\alpha$ is a conversion coefficient from coke concentration $C_k$ to active site concentration $S$. Taking the limit of $\Delta t$, we get the differential form of the difference eq 8:

$$\frac{dS}{dt} = \alpha\frac{S}{S_0}[-r_d(S_0,C^*)] \quad (9)$$

Substituting eq 3 into eq 9 and integrating, we get the final equation for catalyst deactivation caused by coking:

$$\phi = \exp(-\alpha_C C_k) \quad (10)$$

where $\alpha_C \equiv \alpha/S_0$ is the catalyst deactivation constant. If the catalyst loses all its activity when all the active sites are fully covered with carbon, we can estimate $\alpha_C$. Since the reforming reactions occur on the catalyst surface (mainly internal surface), we assume the active sites are fully covered when all the catalyst pores are fully filled with carbon. For nickel reforming catalysts, typical surface area is 20−66 $m^2/g$ [23−25] and typical micropore mean radius is ∼17 Å.[26] Suppose the catalyst pores are equivalent as cylinders with the same surface area and pore radius, the maximum amount of coke that can be deposited is 0.16 g/g of catalyst. For mathematical simplicity, we assume the catalyst will lose 99% of its activity when the coke content reaches 0.16 g/g of catalyst. Thus, the deactivation constant $\alpha_C$ is 28.8 g of catalyst/g of coke.

### Reaction Kinetics and Reformer Modeling

For steam reforming of heptane, the reactions and their kinetic rate equations are summarized in Table 1. In this paper, we assume the axial dispersion is negligible due to the large gas velocity (∼3 m/s) in the circulating fluidized bed membrane reformer. We also assume a constant average radial flow condition. Then the circulating fluidized bed membrane reformer is modeled as a plug flow reactor with co-current flow in the reactor and membrane sides. The other main assumptions for the CFBMR modeling are as follows: (1) steady-state operation; (2) the slip between the solid and gas phases is negligible due to the use of fine catalyst particles (∼186 $\mu$m) in the circulating fluidized bed; [32] (3) there is no hydrogen oxidation taking place over a nickel reforming catalyst (this assumption is based on the experimental result reported by Roy and co-workers [33]); (4) the palladium-based hydrogen membranes and dense perovskite oxygen membranes are 100% selective for the permeation of the components hydrogen and oxygen; [34−36] (5) the heat capacities of the

**Table 1. Reactions and Their Kinetic Rate Equations**

| reaction | kinetic rate equation | ref |
|---|---|---|
| $C_7H_{16} + 7H_2O \rightarrow 7CO + 15H_2$ | $r_1 = \dfrac{k_1 P_{C_7H_{16}}}{\left[1 + 25.2\dfrac{P_{C_7H_{16}}P_{H_2}}{P_{H_2O}} + 0.077\dfrac{P_{H_2O}}{P_{H_2}}\right]^2}$ | 23 |
| $CO + 3H_2 \rightleftharpoons CH_4 + H_2O$ | $r_2 = k_2\left(\dfrac{P_{CO}{P_{H_2}}^{0.5}}{K_2} - \dfrac{P_{CH_4}P_{H_2O}}{{P_{H_2}}^{2.5}}\right)/\mathrm{DEN}^2$ | |
| $CO + H_2O \rightleftharpoons CO_2 + H_2$ | $r_3 = k_3\left(\dfrac{P_{CO}P_{H_2O}}{P_{H_2}} - \dfrac{P_{CO_2}}{K_3}\right)/\mathrm{DEN}^2$ | 24 |
| $CH_4 + 2H_2O \rightleftharpoons CO_2 + 4H_2$ | $r_4 = k_4\left(\dfrac{P_{CH_4}{P_{H_2O}}^2}{{P_{H_2}}^{3.5}} - \dfrac{P_{CO_2}{P_{H_2}}^{0.5}}{K_2K_3}\right)/\mathrm{DEN}^2$ | |
| $C_7H_{16} + 3.5O_2 \rightarrow 7CO + 8H_2$ | $r_5 = k_5 TP^{0.3}{C_{C_7H_{16}}}^{0.5}C_{O_2}$ | 27 |
| $CH_4 + 2O_2 \rightarrow CO_2 + 2H_2O$ | $r_6 = k_6 P_{CH_4}P_{O_2}$ | |
| $CH_4 + CO_2 \rightleftharpoons 2CO + 2H_2$ | $r_7 = k_7 P_{CH_4}P_{CO_2}\left(1 - \dfrac{{P_{CO}}^2{P_{H_2}}^2}{K_7 P_{CH_4}P_{CO_2}}\right)$ | 28 |
| $C_7H_{16} \rightarrow 7C + 8H_2$ | $r_8 = k_8$ | 15 |
| $CH_4 \rightleftharpoons C + 2H_2$ | $r_9 = \dfrac{k_9 K_{CH_4}\left(P_{CH_4} - \dfrac{{P_{H_2}}^2}{K_{9a}}\right)}{\left(1 + \dfrac{{P_{H_2}}^{1.5}}{K_{9b}} + K_{CH_4}P_{CH_4}\right)^2}$ | 29 |
| $2CO \rightarrow C + CO_2$ | $r_{10} = \dfrac{k_{10}P_{CO}}{\left(1 + K_{10a}P_{CO} + K_{10b}\dfrac{P_{CO_2}}{P_{CO}}\right)^2}$ | 30 |
| $C + H_2O \rightarrow CO + H_2$ | $r_{11} = k_{11}{P_{H_2O}}^{0.5}$ | |
| $C + 0.5O_2 \rightarrow CO$ | $r_{12} = k_{12}{P_{O_2}}^{0.5}$ | 31 |
| $C + CO_2 \rightarrow 2CO$ | $r_{13} = k_{13}{P_{CO_2}}^{0.5}$ | |

where $\mathrm{DEN} = 1 + K_{CO}P_{CO} + K_{H_2}P_{H_2} + K_{CH_4}P_{CH_4} + K_{H_2O}P_{H_2O}/P_{H_2}$

components are constant; (6) the operating pressures in the reactor, hydrogen, and oxygen membrane tubes are constant.

The steady-state equation for material balance in the reaction side is given by

$$\frac{\mathrm{d}F_i}{\mathrm{d}l} = \rho_C(1-\epsilon)A_f\sum_{j=1}^{13}\sigma_{i,j}r_j - aJ_{H_2}\pi N_{H_2}d_{H_2} + bJ_{O_2}\pi N_{O_2}d_{O_2} \quad (11)$$

where $a$ and $b$ are the control indices for the membrane permeation fluxes. For hydrogen, $a = 1$ and $b = 0$; for oxygen, $a = 0$ and $b = 1$; for all other components, $a = 0$ and $b = 0$. In the reaction side, component $i$ ($i = 1, 2, \ldots 8$) stands for heptane, methane, carbon dioxide, carbon monoxide, hydrogen, steam, oxygen, and carbon, respectively.

The energy balance equation for the reformer (including the membrane tubes) is given by

$$\frac{\mathrm{d}T}{\mathrm{d}l} = \frac{\sum_{j=1}^{13} r_j(-\Delta H_j)\rho_C(1-\epsilon)A_f + \dot{Q}}{\sum_{k=1}^{13} F_k Cp_k} \quad (12)$$

Component $k$ ($k = 1, 2, \ldots 13$) stands for heptane, methane, carbon dioxide, carbon monoxide, hydrogen, steam, oxygen, and carbon in the reaction side, hydrogen and sweep gas in hydrogen permselective membrane tubes, oxygen and nitrogen in oxygen permselective membrane tubes, and the circulating solid catalyst, respectively.

The material balance equation in hydrogen permeation membrane tubes is given by

$$\frac{\mathrm{d}F_{H_2,P}}{\mathrm{d}l} = \pi N_{H_2}d_{H_2}J_{H_2} \quad (13)$$

The material balance equation in oxygen permeation membrane tubes is given by

$$\frac{dF_{O_2,P}}{dl} = -\pi N_{O_2} d_{O_2} J_{O_2} \quad (14)$$

The membrane permeation fluxes of hydrogen and oxygen are dependent on the type of membrane. In this preliminary investigation, the hydrogen permselective membrane is assumed that palladium is coated on the ceramic tube (to stand a high operating pressure). Thus, for a palladium-based hydrogen membrane, the hydrogen permeation flux can be calculated using the following equation:[34,35]

$$J_{H_2} = \frac{2.003 \times 10^{-5}}{\delta_{H_2}} \exp\left(\frac{-15700}{RT}\right)\left(\sqrt{p_{H_2,r}} - \sqrt{p_{H_2,p}}\right) \quad \frac{mol}{m^2 \cdot s} \quad (15)$$

For the dense perovskite oxygen membrane, the oxygen permeation flux can be calculated using the following equation:[36]

$$J_{O_2} = 7.339 \times 10^{-7} \exp\left(\frac{-62700}{RT}\right)\frac{T}{\delta_{O_2}} \ln\left(\frac{P_{O_2,p}}{P_{O_2,r}}\right) \quad \frac{mol}{m^2 \cdot s} \quad (16)$$

Because the catalyst deactivation occurs when carbon deposits, the reaction rate equations are reformulated accordingly by introducing the catalyst activity function as follows:

$$r_j = r_{j0}\phi_j \quad (17)$$

where $\phi_j$ is the specific catalyst activity function for the $j$th reaction, which is calculated by eq 10 or equal to 1.0 depending on whether the $j$th reaction is affected by the catalyst deactivation or not. $r_{j0}$ is the initial reaction rate for fresh catalyst as given in Table 1.

## Simulation Results and Discussion

In this investigation, the yield of hydrogen is defined as the total moles of hydrogen produced per mole of heptane fed. Methane yield is defined as the total moles of methane produced per mole of heptane fed. Heptane conversion is defined as the total moles of heptane converted per mole of heptane fed. The steam-to-carbon feed ratio is defined as the feed flow ratio of steam to carbon of heptane. It equals to the steam-to-heptane feed ratio divided by 7 since 1 mol of heptane contains 7 mol of carbon. The base set of simulation parameters and reaction conditions is listed in Table 2. To investigate the effect of hydrogen permselective membranes on hydrogen production and carbon formation, the reformer is simulated under isothermal condition when only hydrogen permselective membranes are used. To investigate the thermal effect of oxygen introduction, the reformer is simulated under nonisothermal (adiabatic) condition when oxygen is introduced through direct feed/oxygen permselective membranes.

**1. Carbon Deposition and Catalyst Deactivation in Isothermal CFBMR.** In the circulating fluidized bed, the catalyst particles are continuously carried out by the gas stream and replaced with fresh or fully regenerated catalysts. For fluid dynamic simplicity, we assume the solid catalyst particles have the same velocity as the gas stream (~3 m/s). The solid fraction in a circulating fluidized bed varys in the range of 0.02−0.22. [39,40] The typical flow rate of heptane used in this investigation is 0.64 kmol/h. If steam reforming of heptane is operated at an extreme condition with complete heptane cracking without any carbon gasification or carbon burning, then the maximum possible carbon content $C_k$ for this case is 0.001 064−0.011 68 g of carbon/g of catalyst. Therefore, the catalyst activity $\phi$ calculated by eq 10 for this extreme condition is 0.714−0.970. However, at typical steam reforming conditions, most of heptane reacts with steam for hydrogen production and only part of heptane cracks to generate carbon. Furthermore, because there is usually excess steam and other gasification agents such as oxygen, hydrogen, or carbon dioxide present in the CFBMR, the carbon content will be less and the catalyst activity will be higher than the lower value of 0.714.

Figure 2 shows the carbon mass flow rate along the length of an isothermal reformer at 823 K as a function of solid catalyst fraction for the case without any hydrogen or oxygen membranes. At the simulation

**Table 2. Base Set of Simulation Parameters and Reaction Conditions**

| | |
|---|---|
| CFBMR Reformer Construction Parameters | |
| length of the reformer and membrane tubes | 2 m |
| inside diameter of the reformer tube [18] | 0.0978 m |
| outside diameter of the reformer tube [18] | 0.1154 m |
| outside diameter of hydrogen membrane tubes [37] | 0.00498 m |
| thickness of palladium layer on hydrogen membranes tubes [34] | 20 $\mu$m |
| total wall thickness of hydrogen membrane tubes [37] | 0.00024 m |
| outside diameter of oxygen membranes tubes | 0.00489 m |
| thickness of dense perovskite film on oxygen membrane tubes [38] | 50 $\mu$m |
| Nickel Steam Reforming Catalyst | |
| catalyst particle density [18] | 2835 kg/m$^3$ |
| mean catalyst particle size [37] | 186 $\mu$m |
| solid fraction of fast fluidization bed [39,40] | 0.2 |
| Process Feeds and Reaction Conditions[23] | |
| feed flow rate of heptane | 0.64 kmol/h |
| feed flow rate of steam | 9 kmol/h |
| feed flow rate of hydrogen | 0.1 kmol/h |
| steam-to-carbon feed ratio | 2 mol/mol |
| reaction temperature | 823 K |
| reaction pressure | 1013 kPa |
| feed flow rate of sweep gas in hydrogen membrane tubes | 1 kmol/h |
| operating pressure in palladium hydrogen membrane tubes | 101.3 kPa |
| feed flow rate of air in oxygen membrane tubes | 10 kmol/h |
| operating pressure in oxygen membrane tubes | 3039 kPa |

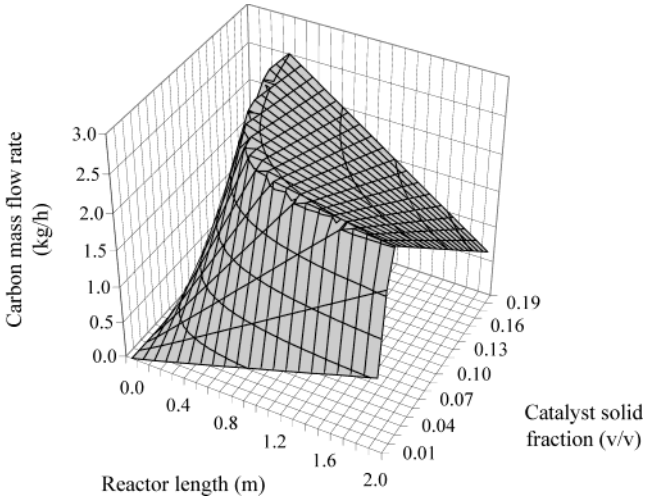


**Figure 2.** Carbon mass flow rate at 823 K for isothermal operation without hydrogen or oxygen membranes (reaction pressure 1013 kPa; steam-to-carbon feed ratio 2 mol/mol).

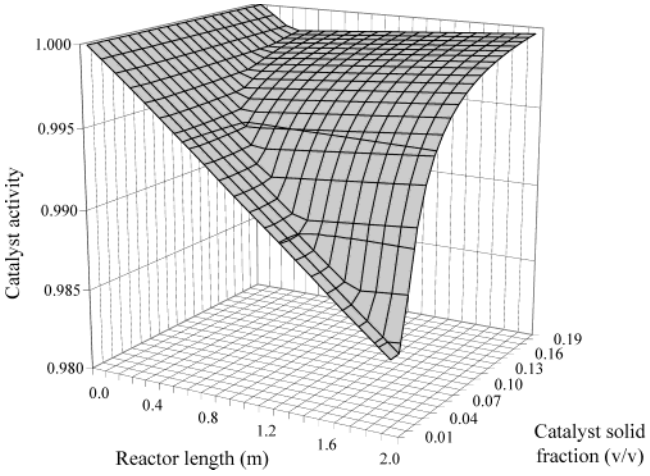


**Figure 3.** Catalyst activity at 823 K for isothermal operation without hydrogen or oxygen membranes (reaction pressure 1013 kPa; steam-to-carbon feed ratio 2 mol/mol).

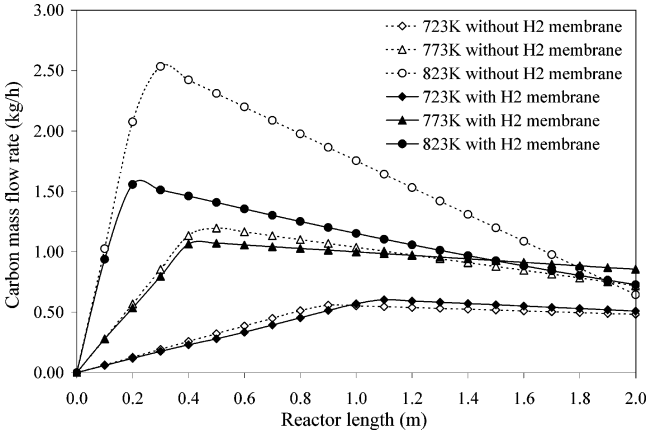


**Figure 4.** Carbon mass flow rate at different temperatures for the cases without and with hydrogen permselective membranes under isothermal conditions (reaction pressure 1013 kPa; steam-to-carbon feed ratio 2 mol/mol).

conditions in Table 2, the carbon mass flow rate or the deposited carbon on the circulating catalyst for the case without any hydrogen or oxygen membranes can be as high as 2.56 kg/h. The carbon mass flow rate increases first along the reactor length and also increases with increase of the solid catalyst fraction in the bed. However, after a certain reactor length or solid catalyst fraction, the carbon mass flow rate decreases. This phenomenon is due to the fact that the carbon formation in the reformer is a catalytic process related to the amount of catalyst. The less of the solid catalyst in the bed, the slower the carbon formation rate from heptane cracking. At the same time, as the steam reforming of heptane proceeds, the byproducts carbon monoxide and methane also contribute to the formation of carbon on the nickel catalyst. Similarly, the less the solid catalyst in the bed, the slower the steam reforming of heptane and the slower the formation of carbon monoxide and methane. As a result the less the solid catalyst, the slower the carbon formation rate from carbon monoxide and methane. Summation of the above factors results in the fact that the carbon formation rate increases when the solid catalyst fraction increases and vice versa. However, when the solid catalyst fraction is high, the steam reforming rate of heptane is high, which makes the reactor length for complete heptane conversion short. After the complete conversion of heptane at a certain reactor length, the major source of carbon formation from heptane stops. On the other hand, carbon gasification by steam, hydrogen, and carbon dioxide in the reformer continues. As a result, the overall carbon deposition decreases, making the carbon mass flow rate decrease along the rest of the reactor length shown in Figure 2. For example, at a solid catalyst fraction of 0.2, the maximum carbon mass flow rate is at the reactor length of 0.3 m. This position is the place where heptane is fully converted to hydrogen and carbon monoxide in the steam reformer (see later Figure 5). From the results shown in Figure 2, the maximum carbon mass flow rate in the bed (2.56 kg/h) for the case without any hydrogen or oxygen membranes at 823 K is at a solid catalyst fraction close to 0.05 v/v. The carbon mass flow rate increases when the solid catalyst fraction increases from 0 to 0.05 v/v, and then it decreases after the solid catalyst fraction of 0.05 v/v.

Figure 3 shows the catalyst activity as a function of the solid catalyst fraction in the bed. Although the carbon mass flow rate in the bed can be as high as 2.56 kg/h, the catalyst activity is almost constant (in the range of 0.984−1.0). As defined by eq 10, the catalyst activity is the function of carbon content on the catalyst. High carbon content on the catalyst increases the catalyst deactivation and reduces the catalyst activity. However, in our novel circulating reformer configuration, the mass ratio of circulating solid catalyst to carbon is high. Furthermore, the catalyst is continuously regenerated along the circulation using excess air. As a result, although the carbon deposition is high, the carbon content on the catalyst in the circulating fluidized bed is still small, making the catalyst activity high. The surface shown in Figure 3 shows that the catalyst activity may slightly increase along the length of the reactor with the increase of catalyst solid fraction. This is because the amount of circulating catalyst increases when the catalyst solid fraction in the bed increases. The increase of the amount of catalyst decreases the carbon content on the nickel reforming catalyst. As a result, the catalyst activity increases slightly. Obviously this is a potential advantage of the circulating fluidized bed over conventional fixed-bed steam reformers.

**2. Effect of Reaction Temperature.** Figure 4 shows the carbon mass flow rate in the range 723−823 K for the cases without and with hydrogen permselective

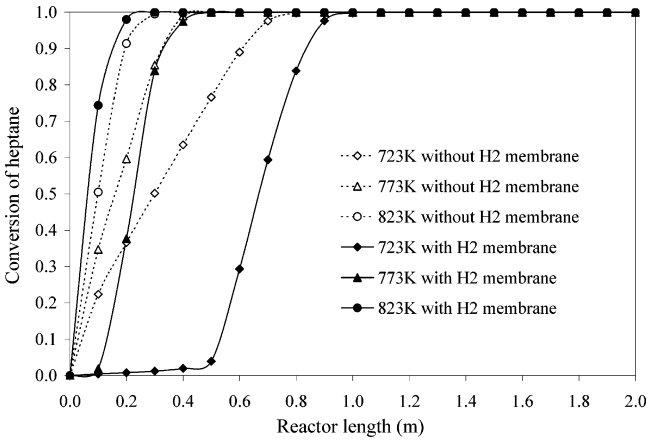


**Figure 5.** Heptane conversion at different temperatures for the cases without and with hydrogen permselective membranes under isothermal conditions (reaction pressure 1013 kPa; steam-to-carbon feed ratio 2 mol/mol).

membranes. The number of hydrogen membrane tubes is 20, and the solid fraction in the circulating fluidized bed is 0.2 v/v. For both cases without and with hydrogen membranes, the carbon mass flow rate increases first and then decreases along the reactor length. As mentioned earlier, the development of maximum carbon mass flow rate in the bed is due to the complete conversion of heptane (Figure 5). For example, for the case without hydrogen membranes at 823 K, heptane is fully converted at the reactor length of 0.3 m corresponding to the maximum carbon mass flow rate shown in Figure 4. Since the major source of carbon formation is the catalytic cracking of heptane, the complete consumption of heptane makes carbon formation from heptane stop. On the other hand, carbon gasification by steam, hydrogen, and carbon dioxide continues. As a result the carbon mass flow rate (the overall carbon deposited on the catalyst) decreases along the rest of the reactor length.

For the case with hydrogen permselecvtive membranes, the carbon mass flow rate in the bed is lower than the case without hydrogen permselective membranes. This interesting phenomenon can be explained by the effects of the removal of product hydrogen using hydrogen permselective membranes from the following three aspects: First, the removal of hydrogen from the reaction side decreases the partial pressure of hydrogen. Figure 6 shows that the reaction rate of heptane steam reforming is non-monotonic with respect to hydrogen partial pressure. The rate of heptane steam reforming increases as the partial pressure of hydrogen increases from 0 to 25.3 kPa and then decreases as the partial pressure of hydrogen increases above 25.3 kPa. For most of the cases investigated, the partial pressure of hydrogen is much higher than 25.3 kPa. Since the removal of hydrogen using hydrogen permselective membranes decreases the partial pressure of hydrogen, it increases the rate of heptane steam reforming, resulting in a higher conversion of heptane and a higher reaction rate ratio of steam reforming to carbon formation from heptane. As a result, the reactor length for complete heptane conversion shown in Figure 5 is shorter and the total amount of carbon formed from heptane is smaller. Second, although the removal of hydrogen using hydrogen permselective membranes may also shift the carbon formation from methane cracking, it shifts the reversible reforming reactions, especially steam reforming of methane, to the direction for hydrogen production, making the concentration of methane much lower, as shown in Table 3. Since methane is the second important source for carbon formation in the heptane steam reforming system, the lower the concentration of methane, the lower the carbon formation from the byproduct methane. Third, because the removal of hydrogen shifts the reversible reactions and breaks the thermodynamic

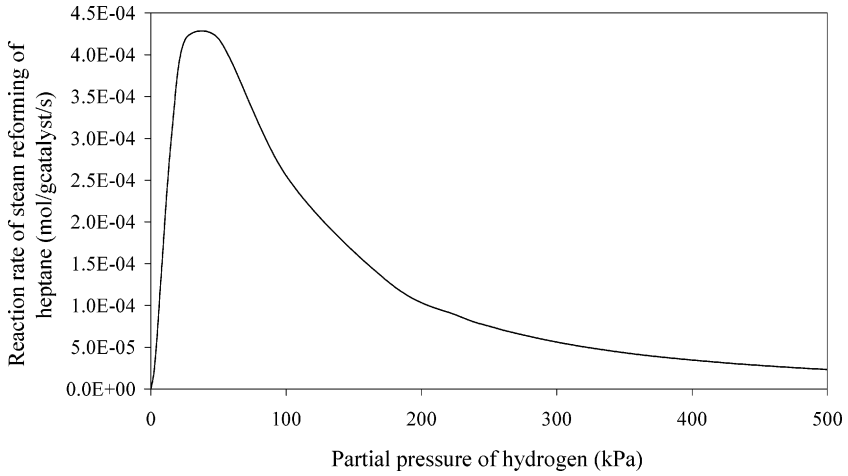


**Figure 6.** Steam reforming rate of heptane as a function of the partial pressure of hydrogen.

**Table 3. Methane Yield and Hydrogen Yield at Different Temperatures for the Isothermal Cases without and with Hydrogen Membranes (Reaction Pressure 1013 kPa, Steam-to-Carbon Feed Ratio 2 mol/mol)**

| | without hydrogen membranes | | with hydrogen membranes | | |
|---|---|---|---|---|---|
| temp (K) | methane yield | hydrogen yield | methane yield | hydrogen yield | improvement of hydrogen yield (%) |
| 723 | 5.084 | 1.503 | 2.069 | 13.515 | 799 |
| 773 | 4.813 | 2.464 | 1.098 | 17.181 | 597 |
| 823 | 4.475 | 3.700 | 0.502 | 19.340 | 423 |

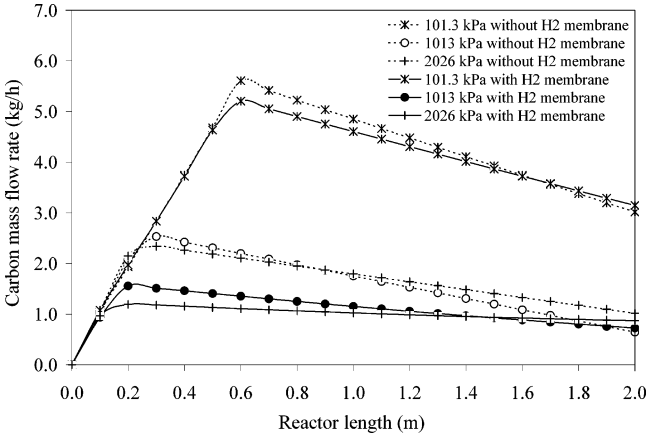


**Figure 7.** Carbon mass flow rate at different reaction pressures for the cases without and with hydrogen permselective membranes under isothermal condition (reaction temperature 823 K; steam-to-carbon feed ratio 2 mol/mol).

equilibrium limitation, the need of a high steam-to-carbon feed ratio for these reforming reactions is less important. On the other hand, because steam can gasify the deposited carbon on the catalyst, the overall carbon deposition is controlled when excess steam is used.

Figure 5 shows that for the case with hydrogen permselective membranes the conversion of heptane at 723 K is lower than the case without hydrogen membranes. This is due to the low partial pressure of hydrogen at the entrance of the reformer (feed partial pressure of hydrogen is 10.4 kPa). The removal of hydrogen decreases the partial pressure of hydrogen. Then the hydrogen production rate at 723 K is relatively slow according to Figure 6. Therefore the removal of hydrogen at 723 K retards the steam reforming of heptane near the entrance of the reformer. As a result, the position of heptane full conversion and the maximum carbon mass flow rate occur with a longer reactor length compared to the case without hydrogen membranes.

As shown in Table 3, without hydrogen permselective membranes, the yield of byproduct methane is high and the yield of hydrogen is low. However, with hydrogen permselective membranes, the yield of methane is significantly reduced and the yield of hydrogen is simultaneously enhanced. For example, at 823 K without hydrogen membranes, the methane yield is 4.475 (mol/mol of heptane fed) and hydrogen yield is 3.700 (mol/mol of heptane fed). When hydrogen membranes are used, the methane yield decreases to 0.502 (mol/mol of heptane fed) and hydrogen yield increases to 19.340 (mol/mol of heptane fed). The improvements of hydrogen yield and productivity using hydrogen permselective membranes are significant, about 423 and 799% for 823 and 723 K, respectively. Thus, the use of hydrogen permselective membranes has potential advantages not only to enhance the production of hydrogen but also to limit the deposition of carbon in this novel circulating fluidized bed membrane reformer.

**3. Effect of Reaction Pressure.** Figure 7 shows the effect of reaction pressure on the carbon deposition at 823 K. Similar to previous results, the maximum carbon mass flow rate develops at the position where heptane is fully converted. For both cases without and with hydrogen permselective membranes, the carbon mass flow rate decreases as the reaction pressure increases. This is because at the same steam-to-carbon (of heptane) feed ratio, the higher the reaction pressure, the higher the partial pressure of steam in the reforming system and therefore the faster the carbon gasification by steam. Since steam is the major feed in the gas stream, carbon gasification by steam is more important than the other gasification by hydrogen and carbon dioxide. As mentioned earlier, with hydrogen permselective membranes, the overall carbon deposition is suppressed to lower values. Figure 7 also shows that there is a shift in location of complete heptane conversion for higher pressure and with hydrogen membrane. This phenomenon is not observed at a lower pressure such as 101.3 kPa. Similarly, as discussed in a previous section, at 823 K, the partial pressure of hydrogen in the reaction bed is higher than 25.3 kPa. The removal of hydrogen using hydrogen permselective membranes decreases the partial pressure of hydrogen and it increases the rate of heptane steam reforming, resulting in a higher conversion of heptane and a higher reaction rate ratio of steam reforming to carbon formation from heptane. For high reaction pressure, the removal of hydrogen is enhanced since the partial pressure difference of hydrogen between the reaction bed and membrane tubes is larger. As a result, there is a shift in location of complete heptane conversion for higher pressure and with a hydrogen membrane. However, for lower pressure such as 101.3 kPa, the partial pressure difference for hydrogen permeation is rather small. As a result, the effect of hydrogen removal on heptane conversion and carbon deposition is small.

Table 4 shows that the yield of methane increases when the reaction pressure increases while the yield of hydrogen decreases for the case without hydrogen permselective membranes. However, for the case with hydrogen membranes, the yield of methane decreases and the yield of hydrogen increases with the increase of reaction pressure. Because steam reforming of hydrocarbons is characterized by an increase in the number of moles, the high reaction pressure limits the production of hydrogen. However, when the hydrogen membranes are used, the removal of hydrogen shifts the reversible reactions, mainly methanation and water gas shift reactions, to the direction for hydrogen production and therefore "breaks" the thermodynamic equilibrium barrier in the reforming system. Furthermore, high reaction pressure increases the hydrogen partial pres-

**Table 4. Methane Yield and Hydrogen Yield at Different Reaction Pressures for the Isothermal Cases without and with Hydrogen Membranes (Reaction Temperature 823 K, Steam-to-Carbon Feed Ratio 2 mol/mol)**

| | without hydrogen membranes | | with hydrogen membranes | | |
|---|---|---|---|---|---|
| reaction pressure (kPa) | methane yield | hydrogen yield | methane yield | hydrogen yield | improvement of hydrogen yield (%) |
| 101.3 | 2.732 | 9.349 | 1.672 | 13.394 | 43 |
| 1013 | 4.475 | 3.699 | 0.502 | 19.340 | 423 |
| 2026 | 4.718 | 2.711 | 0.268 | 20.362 | 651 |

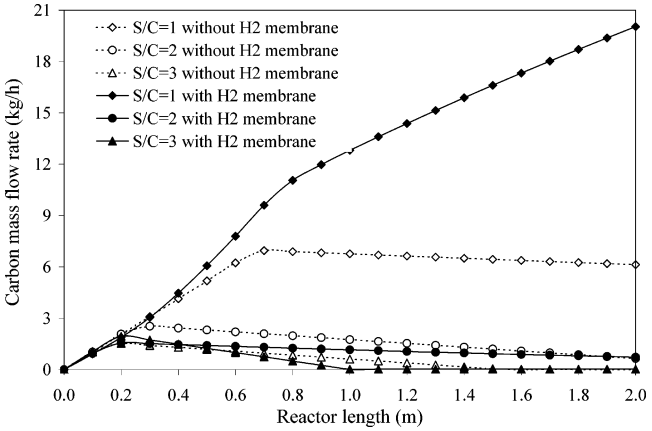


**Figure 8.** Carbon mass flow rate at different steam-to-carbon ratios for the cases without and with hydrogen permselective membranes under isothermal condition (reaction temperature 823 K; reaction pressure 1013 kPa, S/C in legend stands for the steam-to-carbon feed ratio).

sure difference between the reaction side and membrane tubes, making the hydrogen permeation flux high.

**4. Effect of Steam-to-Carbon Feed Ratio.** Figure 8 shows the effect of steam-to-carbon feed ratio on the carbon deposition at 823 K and 1013 kPa for an isothermal CFBMR. For both cases without and with hydrogen permselective membranes, the carbon mass flow rate in the bed increases when steam-to-carbon feed ratio decreases. At a steam-to-carbon feed ratio of 2 or 3 mol/mol, the carbon mass flow rate with hydrogen permselective membranes is lower than the case without hydrogen permselective membranes. However, at a low steam-to-carbon feed ratio of 1 mol/mol, the carbon mass flow rate with hydrogen permselective membranes is higher and keeps increasing along the reactor length even after complete heptane conversion at a reactor length of 0.8 m. This phenomenon can be explained by dividing the steam-to-carbon feed ratios into two regions: high and low steam-to-carbon feed ratio regions. For the high steam-to-carbon feed ratio region, for example, 2 or 3 mol/mol, the explanation for the carbon deposition in the bed is similar to the earlier cases. While for the low steam-to-carbon feed ratio region, for example, 1 mol/mol, the steam feed in the reformer is not excess for the steam reforming of heptane and methane since the stoichiometric coefficient of steam reforming of heptane in Table 1 is 7 (the minimum steam-to-carbon feed ratio is 1 mol/mol). Without hydrogen permselective membranes, the thermodynamic equilibrium limits the hydrogen production and the methanation reaction produces a lot of methane (4.726 mol/mol of heptane fed in Table 5). As a result, the conversion of steam is not high, ~0.49 (mol/mol fed) since the methanation reaction also produces some steam. However, when hydrogen permselective membranes are used, the removal of hydrogen decreases the partial pressure of hydrogen and increases the rate of steam reforming of heptane shown in Figure 6. Thus, the reaction ratio of steam reforming to carbon formation from heptane is higher. At the same time, the removal of hydrogen shifts the reversible reactions, steam reforming of methane, water gas shift, and methane cracking reactions, to the direction for hydrogen production. As a result, the conversion of steam is very high, ~0.96 (mol/mol fed). It is also found that steam is fast consumed near the reactor length where heptane is fully converted. Table 5 shows that at a low steam-to-carbon ratio of 1 mol/mol, the exit methane yield is still very high, ~2.014 (mol/mol of heptane fed). This fact implies that after the high conversion of steam and the full conversion of heptane, the only main reaction is reversible methane cracking. The continuous removal of hydrogen using hydrogen permselective membranes enhances the methane cracking for carbon formation. Thus, the carbon mass flow rate shown in Figure 8 keeps increasing for the case with a low steam-to-carbon feed ratio of 1 mol/mol. Although the exit carbon mass flow rate can be as high as 20 kg/h, the catalyst activity is still high at 0.9877. This is due to the high mass flow ratio of solid catalyst to gas stream in the bed and the continuous catalyst regeneration during the catalyst circulation. Figure 8 also shows that at a high steam-to-carbon feed ratio, for example, 3 mol/mol, the exit carbon mass flow rate is zero. Thus, the deposited carbon on the catalyst is completely gasified before exiting the CFBMR. This implies that at certain high steam-to-carbon feed ratio the exit carbon deposition-free operation could be achieved. In the present investigation, the carbon deposition-free operation can be reached at a minimum/critical steam-to-carbon feed ratio of 2.5 mol/mol (roughly) for both cases without and with hydrogen permselective membranes. Table 5 shows that the methane yield decreases and the hydrogen yield increases when the steam-to-carbon feed ratio increases both without and with hydrogen membranes.

**5. Effect of Oxygen Introduction on the Adiabatic CFBMR.** In this section, in order to investigate the thermal effect of the oxygen introduction, the CFBMR is investigated under adiabatic instead of isothermal conditions. The oxygen is supplied by direct feed or through oxygen permselective membranes where air is fed. Five adiabatic bed configurations are considered: (1) without any hydrogen or oxygen membranes; (2) with 20 hydrogen membrane tubes only; (3) with 20 hydrogen and 80 oxygen membrane tubes; (4) 0.99 kmol/h direct oxygen feed and with 20 hydrogen membrane tubes; and (5) 0.89 kmol/h direct oxygen feed and with 20 hydrogen and 80 oxygen membrane tubes. The feed temperature is 823 K, the reaction pressure is 1013 kPa, and the steam-to-carbon feed ratio is 2 mol/mol.

Figure 9 shows the carbon mass flow rate for these five adiabatic bed configurations. Similar to the earlier isothermal cases, the carbon mass flow rate first in-

**Table 5. Methane Yield and Hydrogen Yield at Different Steam-to-Carbon Feed Ratios for the Isothermal Cases without and with Hydrogen Membranes (Reaction Temperature 823 K, Reaction Pressure 1013 kPa)**

| | without hydrogen membranes | | with hydrogen membranes | | |
|---|---|---|---|---|---|
| steam-to-carbon feed ratio (mol/mol) | methane yield | hydrogen yield | methane yield | hydrogen yield | improvement of hydrogen yield (%) |
| 1 | 4.726 | 1.944 | 2.014 | 10.532 | 442 |
| 2 | 4.475 | 3.699 | 0.502 | 19.340 | 423 |
| 3 | 4.188 | 5.211 | 0.507 | 21.617 | 315 |

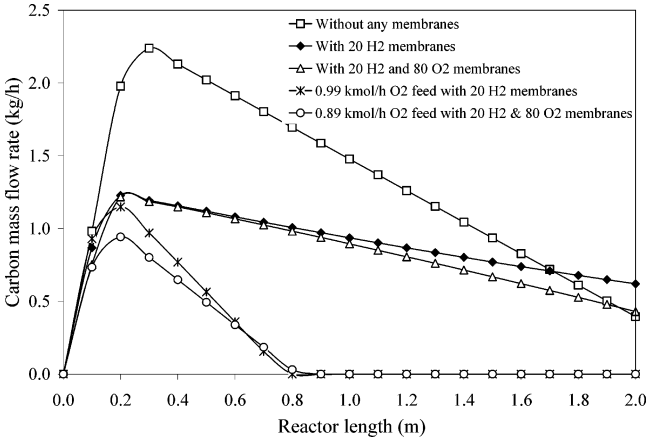


**Figure 9.** Effect of oxygen introduction on the carbon mass flow rate for adiabatic operation (feed temperature 823 K; reaction pressure 1013 kPa; steam-to-carbon feed ratio 2mol/mol).

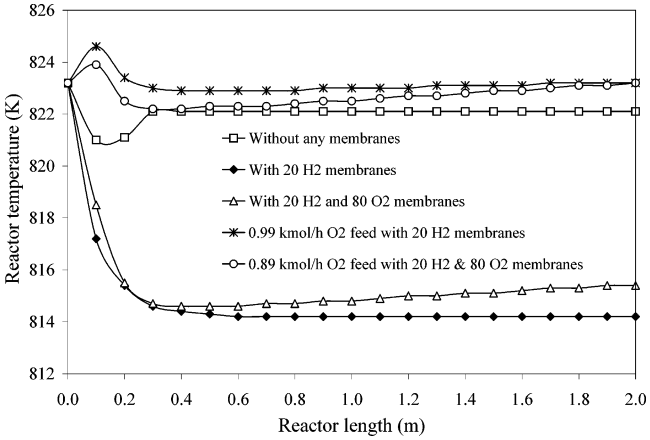


**Figure 10.** Effect of oxygen introduction on reactor temperature profile for adiabatic operation (feed temperature 823 K; reaction pressure 1013 kPa; steam-to-carbon feed ratio 2mol/mol).

creases along the reactor length and then decreases after the full conversion of heptane. Without any hydrogen or oxygen membranes (configuration 1), the maximum carbon mass flow rate developed in the reformer is the highest among these five configurations. With hydrogen permselective membranes, the carbon deposition is suppressed by enhancing the steam reforming of heptane and by shifting the reversible reactions to hydrogen production at a steam-to-carbon feed ratio of 2 mol/mol. With oxygen permselective membranes, the permeated oxygen reacts with heptane and byproduct methane. At the same time, oxygen also reacts with the deposited carbon for gasification, making the overall carbon deposition lower than the case with hydrogen membranes only, especially after complete heptane conversion (configuration 2). The total amount of oxygen permeated from the oxygen membranes into the adiabatic CFBMR for configuration 3 is 0.0324 mol/s (or 0.117 kmol/h). Accordingly, the average oxygen permeation rate is 0.0132 mol $m^{-2}$ $s^{-1}$. However, when oxygen is introduced directly with the feed, the carbon mass flow rate in the bed decreases to zero before exiting the reformer. This is not only because part of the heptane is used for oxidative reforming as well as steam reforming, which decreases the carbon formation from hepatne, but also because of the burning of carbon by oxygen. With oxygen introduction by direct feed or through oxygen permselective membranes, some heptane and byproduct methane are used for exothermic oxidative reforming and supply the heat for the endothermic steam reforming. As a result, the yield of hydrogen shown in Table 6 is slightly lower than the case without any oxygen introduction. However, the reactor temperature profile is improved to autothermal shown in Figure 10. Table 6 shows the hydrogen yield and heptane conversion for these five configurations. From the viewpoint of the yield of hydrogen, the best configuration is configuration 2, while it is very close to that of configuration 3. But the carbon mass flow rate for this case is higher than all the other cases except configuration 1. Due to the fast endothermic steam reforming of heptane and methane, a larger temperature drop shown in Figure 10 develops near the entrance of the reformer, which means larger energy consumption is demanded. However, the introduction of oxygen by direct oxygen feed or through oxygen permselective membranes (configurations 4 and 5) improves the thermal situation considerably. The exothermic oxidative reforming of heptane and methane supplies the heat needed for endothermic steam reforming of the hydrocarbons, making it possible to operate the novel CFBMR reformer autothermally. The penalty for oxygen introduction is a slight decrease in hydrogen yield. However, since the energy supply efficiency is 100% for this in-site heat supply by oxidative reforming of hydrocarbons, this approach has a strong potential as an energy-saving process. Figure 10 shows clearly that the reactor approaches almost the isothermal conditions at a reactor length of 0.3 m. One may say that oxygen has no influence beyond this length and the main role of oxygen is to supply heat in the nonisothermal part at the beginning of the reactor. In this investigation,

**Table 6. CFBMR Performances under Five Adiabatic Bed Configurations (Feed Temperature 823 K, Reaction Pressure 1013 kPa, Steam-to-Carbon Feed Ratio 2 mol/mol).**

| | reformer performance | | |
|---|---|---|---|
| bed configurations | hydrogen yield (mol/mol of heptane fed) | heptane conversion (%) | average oxygen permeation rate (mol $m^{-2}$ $s^{-1}$) |
| without any membranes (configuration 1) | 3.663 | 100 | / |
| with 20 $H_2$ membrane tubes (configuration 2) | 19.046 | 100 | / |
| with 20 $H_2$ and 80 $O_2$ membrane tubes (configuration 3) | 19.033 | 100 | 0.0132 |
| 0.99 kmol/h $O_2$ feed with 20 $H_2$ membrane tubes (configuration 4) | 17.824 | 100 | / |
| 0.89 kmol/h $O_2$ feed with 20 $H_2$ and 80 $O_2$ membrane tubes (configuration 5) | 17.850 | 100 | 0.0123 |

the main role of oxygen introduction into the reformer is to supply the heat from exothermic reforming of hydrocarbon and carbon oxidation. The oxygen in the feed reacts with hydrocarbon and carbon quickly near the entrance of the reformer. The oxygen introduction through membrane permeation still has influence on the reforming system beyond 0.3 m because Figure 9 shows that the carbon mass flow rate decreases after 0.3 m in the reforming bed. It implies that the oxygen permeated through the oxygen membranes reacts with the deposited carbon for carbon oxidation, which decreases the overall carbon deposition on the catalyst and also supplies part of heat for the endothermic reforming reactions. The reactor approaches almost isothermal conditions because of the high mass ratio of solid catalyst to gas stream and the low oxygen permeation flux around 823 K. The high heat capacity ratio of solid catalyst to gas makes the temperature profile flat after the full conversion of oxygen in the feed. Thus, one of the important roles of the circulating solid catalyst in the bed is as a heat carrier for the endothermic reforming reactions.

## Conclusions

This investigation highlights the advantages of the novel circulating fluidized bed reformer with and without hydrogen and oxygen permselective membranes. An exponential catalyst deactivation model equation is developed based on the random carbon deposition mechanism. The results show that although the overall carbon deposition on the catalyst is large, the catalyst activity is still high (close to 1.0) because of the high mass flow ratio of solid catalyst to gas stream and the continuous catalyst regeneration in the novel process. The use of hydrogen permselective membranes breaks the thermodynamic equilibrium barriers and enhances hydrogen production significantly. When the steam-to-carbon feed ratio is high, the use of hydrogen permselective membranes also limits the carbon deposition on the reforming catalyst. However, if the steam-to-carbon feed ratio is low (e.g., 1 mol/mol), the use of hydrogen permselective membranes increases carbon deposition because the removal of hydrogen shifts the reversible methane cracking reaction to carbon formation. Carbon formation increases with the increase of reaction temperature while it decreases with the increase of reaction pressure and the steam-to-carbon feed ratio. The deposited carbon may be efficiently gasified by excess steam (steam-to-carbon feed ratio of >2.5 mol/mol), hydrogen, carbon dioxide or oxygen, making carbon-free operation practically possible. Through the oxygen permselective membranes, with oxygen direct feed, or with both, autothermal operation can be achieved with near-isothermal operating condition, high heptane conversion, and hydrogen yield.

## Acknowledgment

This work was financially supported by Auburn University, Grant 2-12085.

## Nomenclature

*Symbols*

$a$, $b$ = control indices for the membranes fluxes of hydrogen and oxygen components
$A_f$ = free cross-section area of the reactor ($m^2$)
$C^*$ = concentration of protocoke on the catalyst (g/g of catalyst)
$C_i$ = molar concentration of component $i$ ($mol/m^3$)
$C_k$ = concentration of deposited coke on the catalyst (g/g of catalyst)
$Cp_k$ = specific heat of component $k$ ($J\ mol^{-1}\ ^{-1}$)
$d_{H_2}$, $d_{O_2}$ = outside diameters of hydrogen and oxygen membrane tubes (m)
DEN = DEN term, which is given in Table 1
$F_i$ = molar flow rate of component $i$ in the reaction side (mol/s)
$F_k$ = molar flow rate of component $k$ in the reformer, including the reaction side (mol/s)
$\Delta H_j$ = heat of reaction for the $j$th reaction (J/mol)
$J_{H_2}$, $J_{O_2}$ = permeation fluxes of hydrogen and oxygen ($mol\ m^{-2}s^{-1}$)
$k_j$ = generalized (forward) reaction rate constant for the $j$th (reversible) reaction
$K_i$ = absorption constants of component $i$
$K_j$ = reaction equilibrium constant of the $j$th reaction
$l$ = length of reactor (m)
$N_{H_2}$, $N_{O_2}$ = number of hydrogen and oxygen membrane tubes
$P$ = reaction pressure (kPa)
$P_i$ = partial pressure of component $i$ (kPa)
$\dot{Q}$ = rate of heating along the reactor length ($J\ s^{-1}\ m^{-1}$)
$r$, $r_d$ = protocoke formation rate and coke deposition rate ($g\ (g\ of\ catalyst)^{-1}\ s^{-1}$)
$r_j$ = generalized reaction rates ($mol\ (g\ of\ catalyst)^{-1}\ s^{-1}$)
$r_{j0}$ = generalized reaction rates without any catalyst deactivation ($mol\ (g\ of\ catalyst)^{-1}\ s^{-1}$)
$R$ = gas constant ($8.314\ J\ mol^{-1}\ K^{-1}$)
$S$, $S_0$ = concentrations of active sites per gram of catalyst at reaction time $t$ and initially
$t$ = time (s)
$T$ = temperature (K)
$W_{cat}$ catalyst weight (g)

*Greek letters*

$\alpha$ = conversion coefficient from coke concentration to active site concentration of catalyst
$\alpha_C$ = deactivation constant (g of catalyst/g of coke)
$\delta_i$ = thickness of hydrogen or oxygen membranes ($i$ = $H_2$,$O_2$) (m)
$\epsilon$ = void fraction
$\pi$ = 3.141 592 6
$\rho_c$ = density of catalyst ($kg/m^3$)
$\sigma_{i,j}$ = stoichiometric coefficient of component $i$ for the $j$th reaction
$\phi$ = catalyst activity function

## Literature Cited

(1) Armor, J. N. Review: The Multiple Roles for Catalysis in the Production of $H_2$. *Appl. Catal., A* **1999**, *176*, 159−176.

(2) Ohi, J. Hydrogen Energy Futures: Scenario Planning by the U.S. DOE Hydrogen Technical Advisory Panel. *Proceeding of the 14th World Hydrogen Energy Conference*, Montreal, Canada, June 9−13, 2002.

(3) Scholz, W. H. Processes for Industrial Production of Hydrogen and Associated Environmental Effects. *Gas Sep, Purif.* **1993**, *7*, 131−139.

(4) Twigg, M. V., Ed. *Catalyst Handbook*, 2nd ed.; Wolfe Publishing Ltd.: London, 1989; pp 225−282.

(5) Rostrup-Nielsen, J. Hydrogen via Steam Reforming of Naphtha. *Chem. Eng. Prog.* **1977**, *9*, 87−92.

(6) Christensen, T. S. Adiabatic Prereforming of Hydrocarbons−An Important Step in Syngas Production. *Appl. Catal., A* **1996**, *138*, 285−309.

(7) Rostrup-Nielsen, J. R. Industrial Relevance of Coking. *Catal. Today* **1997**, *37*, 225−232.

(8) Yamazaki, O.; Tomishige, K.; Fujimoto, K. Development of Highly Stable Nickel Catalyst for Methane-Steam Reaction under Low Steam to Carbon Ratio. *Appl. Catal., A* **1996**, *136*, 49−56.

(9) Borowiecki, T.; Stasińska, B.; Gołębiowski, A. Effects of Small $MoO_3$ Additions on the Properties of Nickel Catalysts for the Steam Reforming of Hydrocarbons. *Appl. Catal., A* **1997**, 141−156.

(10) Forzatti, P.; Lietti, L. Catalyst Deactivation. *Catal. Today* **1999**, *52*, 165−181.

(11) Trimm, D. L. Catalysts for the Control of Coking during Steam Reforming. *Catal. Today* **1999**, *49*, 3−10.

(12) Kepinski, L.; Stasinska, B.; Borowiecki, T. Carbon Deposition on $Ni/Al_2O_3$ Catalysts Doped with Small Amounts of Molybdenum *Carbon* **2000**, *38*, 1845−185.

(13) Bartholomew, C. H. Mechanisms of Catalyst Deactivation. *Appl. Catal., A* **2001**, *212*, 17−60.

(14) Olsbye, U.; Moen, O.; Slagtern, Å; Dahl, I. M. An Investigation of the Coking Properties of Fixed and Fluid Bed Reactors during Methane-to-Synthesis Gas Reactions. *Appl. Catal., A* **2002**, *228*, 289−303.

(15) Rostrup-Nielsen, J. R. Coking on Nickel Catalysts for Steam Reforming of Hydrocarbons. *J. Catal.* **1974**, *33*, 184−201.

(16) Borowiecki, T. Nickel Catalysts for Steam Reforming of Hydrocarbons: Direct and Indirect Factors Affecting the Coking Rate. *App. Catal.* **1987**, *31*, 207−220.

(17) Rostrup-Nielsen, J. R. *Symposium on the Science of Catalysis and Its Application in Industry*, Sindri, India, 1979; pp 22−24.

(18) Elnashaie, S. S. E. H.; Elshishini, S. S. *Modelling, Simulation and Optimization of Industrial Fixed Bed Catalytic Reactors*; Gordon and Breach Science Publishers: London, 1993.

(19) Chen, Z.; Prasad, P.; Elnashaie, S. S. E. H. The Coupling of Catalytic Steam Reforming and Oxidative Reforming of Methane to Produce Pure Hydrogen in a Novel Circulating Fast Fluidized Bed Membrane Reformer. *Fuel Chem. Div. Prepr.* **2002**, *47* (1), 111−113.

(20) Chen, Z.; Elnashaie, S. S. E. H. Efficient Production of Hydrogen from Higher Hydrocarbons using Novel Membrane Reformer. In *Proceeding of the 14th World Hydrogen Energy Conference*, Montreal, Canada, 2002.

(21) Prasad, P.; Elnashaie, S. Novel Membrane Circulating Fluidized Bed Reformer for Efficient Production of Hydrogen from Natural Gas. *Proceeding of the 14th World Hydrogen Energy Conference*, Montreal, Canada, June 9−13, 2002.

(22) Chen, Z.; Yan, Y.; Elnashaie, S. S. E. H. Modeling and Optimization of a Novel Membrane Reformer for Higher Hydrocarbons. *AIChE J.* **2003**, *49* (5), 1250−1265.

(23) Tottrup, P. B. Evaluation of Intrinsic Steam Reforming Kinetic Parameters from Rate Measurements on Full Particle Size. *Appl. Catal.* **1982**, *4*, 377−389.

(24) Xu, J.; Froment, G. F. Methane Steam Reforming, Methanation and Water-Gas Shift: I. Intrinsic Kinetics. *J. AIChE* **1989**, *35* (1), 88−96.

(25) Sehested, J.; Carlsson, A.; Janssens, T. V. W.; Hansen, P. L.; Datye, A. K. Sintering of Nickel Steam-Reforming Catalysts on MgAl2O4 Spinel Supports. *J. Catal.* **2001**, *197*, 200−209.

(26) Biswas, J.; Do, D. D. A Unified Theory of Coking Deactivation in a Catalyst Pellet. *Chem. Eng. J.* **1987**, *36*, 175−191.

(27) Siminski, V. J.; Wright, F. J.; Edelman, R. B.; Economos, C.; Fortune, O. F. Research on Methods of Improving the Combustion Characteristics of Liquid Hydrocarbon Fuels. *AFAPL* TR 72−74, Air Force Aeropropulsion Laboratory, Wright Patterson Air Force Base, OH, February 1972; Vols. I and II.

(28) Jin, W.; Gu, X.; Li, S.; Huang, P.; Xu, N.; Shi, J. Experimental and Simulation Study on a catalyst Packed Tubular Dense Membrane Reactor for Partial Oxidation of Methane to Syngas. *Chem. Eng. Sci.* **2000**, *55*, 2617−2625.

(29) Snoeck, J. W.; Froment, G. F.; Fowles, M. Kinetic Study of the Carbon Filament Formation by Methane Cracking on a Nickel Catalyst. *J. Catal.* **1997**, *169*, 250−262.

(30) Tottrup, P. B. Kinetics of Decomposition of Carbon Monoxide on a Supported Nickel Catalyst. *J. Catal.* **1976**, *42*, 29−36.

(31) Chen, C. X.; Horio, M.; Kojima, T. Numerical Simulation of Entrained Flow Coal Gasifiers. Part I: Modeling of Coal Gasification in an Entrained Flow Gasifier. *Chem. Eng. Sci.* **2000**, *55*, 3861−3874.

(32) Patience, G. S.; Chaouki, J.; Berruti, F.; Wong, R. Scaling considerations for circulating fluidized bed risers. *Powder Technol.* **1992**, *72* (1), 31−37.

(33) Roy, S.; Pruden, B. B.; Adris, A. M.; Lim, C. J.; Grace, J. R. Fluidized Bed Steam Methane Reforming with Oxygen Input. *Chem. Eng. Sci.* **1999**, *54*, 2095.

(34) Shu, B. P. A.; Grandjean, Kaliaguine, S. Methane Steam Reforming in asymmetric Pd- and Pd−Ag/porous SS Membrane Reactor. *Appl. Catal., A* **1994**, *119*, 305−325.

(35) Barbieri, G.; Di Maio, F. P. Simulation of Methane Steam Reforming Process in a catalytic Pd-Membrane Reactor. *Ind. Eng. Chem. Res.* **1997**, *36*, 2121−2127.

(36) Tsai, C. Y.; Dixon, A. G.; Moser, W. R.; Yi, H. M. Dense Perovskite Membrane Reactors for Partial Oxidation of Membrane to Syngas. *J. AIChE* **1997**, *43* (11A), 2741−2750.

(37) Adris, A. M.; Lim, C. J.; Grace, J. R. The Fluidized Bed Membrane Reactor (FBMR) System: A Pilot Scale Experimental Study. *Chem. Eng. Sci.* **1994**, *49*, 5833−5843.

(38) Ritchie, J. T.; Richardson, J. T.; Luss, D. Ceramic Membrane Reactor for Synthesis gas Production. *J. AIChE* **2001**, *47* (9), 2092−2100.

(39) Kunii, D.; Levenspiel, O. Entrainment of Solids from Fluidized Beds: I. Hold-Up of Solids in the Freeboard, II. Operation of Fast Fluidized Beds. *Powder Technol.* **1990**, *61*, 193−206.

(40) Kunii, D.; Levenspiel, O. Circulating Fluidized-Bed Reactors. *Chem. Eng. Sci.* **1997**, *15*, 2471−2484.

*Received for review* October 23, 2003
*Revised manuscript received* January 3, 2004
*Accepted* January 16, 2004

IE034198I